CORA Cork Open Research Archive
Cartlann Taighde Oscailte Chorcaí

Title	Three-wavelength cavity-enhanced albedometer for measuring wavelength-dependent optical properties and single-scattering albedo of aerosols
Authors	Xu, Xuezhe;Zhao, Weixiong;Fang, Bo;Zhou, Jiacheng;Wang, Shuo;Zhang, Weijun;Venables, Dean S.;Chen, Weidong
Publication date	2018-12-10
Original Citation	Xu, X., Zhao, W., Fang, B., Zhou, J., Wang, S., Zhang, W., Venables, D.S. and Chen, W., 2018. Three-wavelength cavity-enhanced albedometer for measuring wavelength-dependent optical properties and single-scattering albedo of aerosols. Optics express, 26(25), pp. 33484-33500. DOI: 10.1364/OE.26.033484
Type of publication	Article (peer-reviewed)
Link to publisher's version	http://www.opticsexpress.org/abstract.cfm?URI=oe-26-25-33484 - 10.1364/OE.26.033484
Rights	© 2018 Optical Society of America under the terms of the OSA Open Access Publishing Agreement - https://creativecommons.org/licenses/by/4.0/
Download date	2026-11-03 02:28:27
Item downloaded from	https://hdl.handle.net/10468/7904

UCC
University College Cork, Ireland
Coláiste na hOllscoile Corcaigh

Research Article | Vol. 26, No. 25 | 10 Dec 2018 | OPTICS EXPRESS 33484
Optics EXPRESS

Three-wavelength cavity-enhanced albedometer for measuring wavelength-dependent optical properties and single-scattering albedo of aerosols

XUEZHE XU,[1,2] WEIXIONG ZHAO,[1,6] BO FANG,[1,2] JIACHENG ZHOU,[1,2] SHUO WANG,[1,2] WEIJUN ZHANG,[1,2,3,7] DEAN S. VENABLES,[4] AND WEIDONG CHEN[5]

[1]*Laboratory of Atmospheric Physico-Chemistry, Anhui Institute of Optics and Fine Mechanics, Chinese Academy of Sciences, Hefei 230031, Anhui, China*
[2]*University of Science and Technology of China, Hefei 230026, Anhui, China*
[3]*School of Environmental Science and Optoelectronic Technology, University of Science and Technology of China, Hefei 230026, Anhui, China*
[4]*School of Chemistry and Environmental Research Institute, University College Cork, Cork, Ireland*
[5]*Laboratoire de Physicochimie de l'Atmosphère, Université du Littoral Côte d'Opale 59140, Dunkerque, France*
[6]*wxzhao@aiofm.ac.cn*
[7]*wjzhang@aiofm.ac.cn*

Abstract: The spectral dependence of aerosol light absorption (α_{abs}) and single-scattering albedo—[ω, defined as the ratio of the scattering (α_{scat}) and extinction coefficients ($\alpha_{ext} = \alpha_{abs} + \alpha_{scat}$)]—has proven effective in classifying dominant aerosol types. It is also helpful in understanding aerosol sources, transformation, climate and environmental effects, testing aerosol models, and improving the retrieval accuracy of satellite and remote sensing data. Despite the significant progress that has been made with measurement of light absorption and ω, many of the reported instruments either operate at a fixed wavelength or can only measure a single optical parameter. Quantitative multi-parameter wavelength-dependent measurement remains a challenge. In this work, a three-wavelength cavity-enhanced albedometer was developed. The albedometer can measure multiple optical parameters, α_{ext}, α_{scat}, α_{abs}, and ω, at λ = 365, 532, and 660 nm, in real time. The instrument's performance was evaluated using four different type laboratory generated aerosols, including polystyrene latex spheres (PSL, non-absorbing); ammonium sulfate (AS, non-absorbing); suwannee river fulvic acid (SRFA, slightly absorbing; a proxy for light absorbing organic aerosol); and nigrosin (strongly absorbing).

© 2018 Optical Society of America under the terms of the OSA Open Access Publishing Agreement

1. Introduction

Aerosol light absorption (α_{abs}) and single-scattering albedo [SSA, ω, defined as the ratio of the scattering coefficient (α_{scat}) to the extinction coefficient ($\alpha_{ext} = \alpha_{abs} + \alpha_{scat}$)] are key inputs in direct radiative forcing (DRF) calculations [1]. Classifying dominant aerosol types, e.g., black carbon, organic carbon, dust, and sulfate, with the spectral dependence of these two parameters is a worthwhile goal [2–5], and this identification is helpful in understanding aerosol sources, transformation, climate and environmental effects, in testing aerosol models, and in improving the retrieval accuracy of satellite and remote sensing data [6]. However, aerosol chemical composition and mixing state is complex and there are still large uncertainties in such identification. A thorough exploration of the spectral dependence of aerosol optical properties (α_{ext}, α_{scat}, α_{abs}, and ω) for different aerosols is thus a key point in developing a robust aerosol classification method [4,5].

#349705 https://doi.org/10.1364/OE.26.033484
Journal © 2018 Received 31 Oct 2018; revised 19 Nov 2018; accepted 23 Nov 2018; published 7 Dec 2018

Optics EXPRESS

In 2009, Moosmüller, Chakrabarty, and Arnott reviewed the methods used for aerosol light absorption measurement [7]. Since then, substantial progress has been made, primarily in the recent advances in photoacoustic spectroscopy (PAS) for absorption measurements, and cavity ring-down (CRDS) and cavity-enhanced (CES) spectroscopy for extinction measurement.

For the PAS technique, aerosol light absorption can be measured directly by converting light into sound (known as photoacoustic effect) [7] with a zero background and with high sensitivity. An extensive list and comparison of the reported detection precisions with PAS instruments were given in [8]. The state-of-the-art precision was 0.08 Mm^{-1} (at λ = 532 nm with 60 s sampling time) [9], and the normally achievable precision was about 0.5-1.5 Mm^{-1}. For wavelength-dependent absorption measurement, Wiegand, Mathews, and Smith [10] developed a UV-Vis photoacoustic spectrometer combining a broadband arc lamp with narrow bandwidth dichroic filters. Light absorption centered at eight wavelengths from 301 to 687 nm could be measured. Photoacoustic spectrometers using an optical parametrical oscillator (OPOs) [11] or a supercontinuum laser source [12], have achieved an even wider spectral range. For multiple optical parameters measurement, Sharma et al. [13] developed a white light supercontinuum laser based multi-wavelength photoacoustic-nephelometer spectrometer. The instrument integrated photoacoustic and nephelometric spectroscopy, allowing measurements of scattering and absorption coefficients at five wavelengths (centered at 417, 475, 542, 607, and 675 nm) by rotating an optical filter wheel.

For the CRDS technique, Langridge et al. [14] developed a multi-channel cavity ring-down spectrometer for measuring aerosol extinction at λ = 405, 532, and 662 nm. For CES, incoherent broadband cavity-enhanced spectroscopy (BBCES) [15–19] has been used for direct broadband measurements of wavelength-resolved aerosol extinction [20,21]. Very recently, Bluvshtein et al. [22] reported an ambient aerosol UV-Vis optical measurement system that combines two BBCES channels (for extinction measurements at 315 – 345 nm and 390 – 420 nm), one CRDS channel (for extinction measurement at 404 nm), one PAS channel (for absorption measurements at 404 nm), and a three-wavelength integrating nephelometer (IN100, AirPhoton, USA, for scattering measurements at 457, 525, and 637 nm).

CRDS [23], BBCES [24,25], and cavity attenuated phase shift spectroscopy (CAPS) [26] have also been combined with integrating spheres (IS) for aerosol albedo measurements. These instruments allow simultaneous in situ measurements of the aerosol scattering and extinction coefficients (and absorption and ω) in an exact same sample volume. These types of instruments hold promise for sensitive measurement of aerosol light absorption and ω. A combination with laser-induced incandescence (LII) for simultaneous measurements of soot mass concentration can further improve the ability for aerosol types' classification [27]. Cavity-based instruments also allow high-quality measurements of aerosol optical properties at high relative humidities (RH) [14,27,28] which pose a problem for the PAS method (where the sample RH should be controlled between 10 and 30% due to the inability accurate correction of the evaporation-induced bias on the PAS signal, and this also leaves an open question and makes PAS not well suited for high RH conditions.) [7,29]. The cavity-based albedometer can help overcome this limitation, and provide a new method for in situ measurement of aerosol light absorption.

Despite significant progress in developing in situ methods, many of the reported instruments measure only a single optical parameter (absorption coefficient or extinction coefficient) or operate at a fixed wavelength. Quantitative measurement of multiple wavelength-dependent parameters under ambient conditions is still a challenge. In this work, we describe a three-wavelength CES-albedometer allowing α_{ext}, α_{scat}, α_{abs}, and ω to be measured in situ and in real time. The instrument operates at λ = 365, 532, and 660 nm. The performance of the new instrument for measuring reference laboratory generated aerosols is presented and discussed.

Optics EXPRESS

2. Experimental section

The specifications and schematic diagram of the CES-albedometer are shown in Table 1 and Fig. 1. There are three channels. Each channel had the same configuration and components. Output from a fiber coupled LED light source was collimated with an SMA air-spaced doublet collimator and passed a bandpass filter before entering the 70 cm long optical cavity. Gas inlets near the mirrors allowed a slow flow of purified air to protect the surfaces of the cavity mirrors. Light exiting the cavity was focused into a fiber and coupled into a CCD spectrometer (Ocean Optics Maya 2000 Pro) equipped with a 100 μm wide slit. The aerosol extinction was measured over 355-395 nm, 515-545 nm, and 650-680 nm with a spectral resolution of 0.1 nm.

Table 1. Spectral characteristics of three-wavelength CES albedometer.

	LED Light source	Spectral region			
		Extinction	Scattering	Absorption	ω
Channel 1	LedEngin LZ1-10UV00, peaked at 365 nm	355-395 nm	Centered at 365 nm (integrated over 356-370 nm)	365 nm	365 nm
Channel 2	LedEngin LZ1-00G102, peaked at 523 nm	515-545 nm	Centered at 532 nm (integrated over 528-537 nm)	532 nm	532 nm
Channel 3	LedEngin LZ1-00R202, peaked at 660 nm	650-680 nm	Centered at 660 nm (integrated over 656-665 nm)	660 nm	660 nm

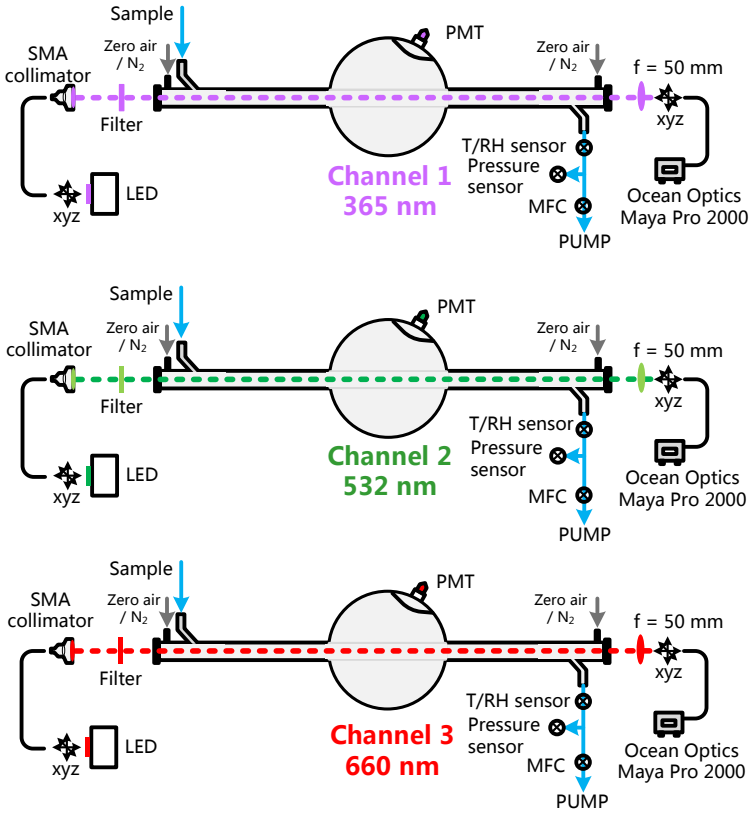


Fig. 1. Schematic diagram of the three-wavelength CES-albedometer. The optical configurations of each channel were identical.

Optics EXPRESS

The optical cavity included an integrating sphere of 15 cm inner diameter and two truncation reduction tubes of 22 cm length and 19 mm inner diameter. The scattering signal was measured with a single channel photomultiplier tube (PMT) [24] and the integrated scattering coefficient was measured directly over the spectral regions of 356-370, 528-537, and 656-665 nm. The extinction and scattering measurements allow calculation of the absorption coefficient and ω at λ = 365, 532, and 660 nm. By using truncation reduction tubes, a small truncation angle (0-1.22°) was achieved, which made a negligible truncated losses (< 0.2%) for particle diameters smaller than 1 μm [24,30].

To shorten the sample residence time and to avoid degrading the IS reflectivity, a 22 cm long quartz tube of 19 mm diameter was inserted within the IS. The flow rates of the sample and purified air near each mirror were 1.3 and 0.1 L min^{-1}, respectively. The sample volume was ~0.3 L and the response time of the instrument was about 20 s (determined by the sample volume of the cavity and the total flow rate).

The CES-albedometer employs BBCES for aerosol optical extinction measurement [18,20,21] and an integrating sphere for scattering measurement [23,24,26,30]. The extinction and scattering coefficients can be express as following equations [23,24,31]:

$$\alpha_{ext}(\lambda) = R_L\left(\frac{1-R(\lambda)}{d}\right)\left(\frac{I_0(\lambda)}{I(\lambda)}-1\right) \tag{1}$$

$$\alpha_{scat} = \frac{I_{scat}}{I_{trans}}\frac{(1-R)}{(1+R)d}\times K = \frac{I_{scat}}{I_{trans}}\times K' \tag{2}$$

where R_L is the ratio of total cavity length (d) to the effective sample length containing the sample when the cavity mirror is purge with gas flow, $R(\lambda)$ is the mirror reflectivity, and $I(\lambda)$ and $I_0(\lambda)$ are the light intensity transmitted through the cavity with and without sample inside the cavity. I_{scat} and I_{trans} are respectively the measured scattering signal with a PMT and the transmitted signal with a CCD spectrometer at the center of the scattering measurement spectral regions. K and K' are the experimentally determined scattering calibration constants.

Optics EXPRESS

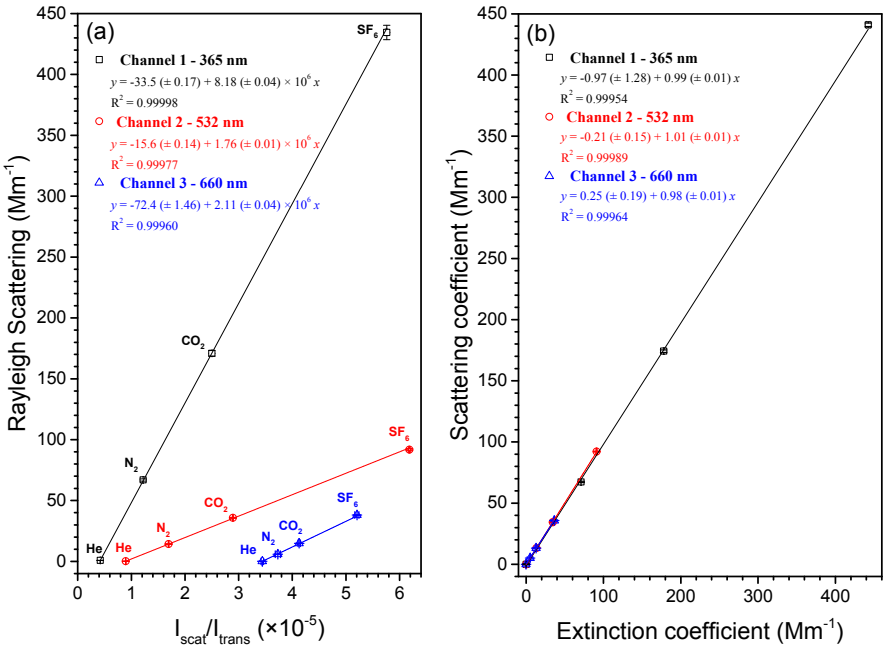


Fig. 2. (a) Calibration of the scattering scaling factor (*K'*) with He, N_2, CO_2 and SF_6 at λ = 365, 532, and 660 nm; (b) Scatter plot of the measured scattering coefficients with integrating sphere and extinction coefficients with BBCES for each channel at three different wavelengths.

The mirror reflectivity $R(\lambda)$ was determined from the Rayleigh scattering of N_2 and CO_2 and the scaling factor (*K'*) were determined from He, N_2, CO_2 and SF_6. More details about the procedure and reference cross sections can be found in [24] and [32] and references therein. $R(\lambda)$ was determined to be 0.99960, 0.99970 and 0.99982 at 365, 532 and 660 nm, respectively. The value of R_L was determined to be 1.05, which led to an effective optical path length of about 1.7, 2.2 and 3.7 km, respectively, for each channel. The scale factor *K'* (account for the differences in scattering light collection efficiency and detector response) was determined from the linear fit of the theoretical Rayleigh scattering coefficients and the measured I_{scat}/I_{trans} ratios (as shown in Fig. 2(a)). The intercepts of I_{scat}/I_{trans} in the figure were considered as the stray light contributed by internal surfaces scattering (e.g. the inner surfaces of the truncation reduction tubes and quartz tube inside the sphere). Excellent correlation between the measured extinction and scattering coefficients for different gases were observed (as shown in Fig. 2(b)), with slopes of 0.99 (± 0.01), 1.01 (± 0.01), and 0.98 (± 0.01) for channel 1 to 3, respectively. In theory, the scattering and extinction should be exactly equal for Rayleigh scattering of the gases. The acceptable unequal in this work was probably caused by the uncertainty associated with the weak scattering coefficients used in the fit.

3. Results and discussion

3.1 Precision, accuracy, and detection limit of developed CES-albedometer

The stability and precision of the CES-albedometer was investigated using an Allan variance analysis [32], as shown in Fig. 3. The optimum average time for each channel ranged from 100 to 1000 s. Continuous time series measurement of α_{ext}, α_{scat}, and α_{abs} at λ = 365, 532, and 660 nm of a particle-free zero air sample are shown in the upper panel of Fig. 3. The time resolutions of each measurement were 12 s (1000 ms integrating time, and 12 spectra averaging), 5 s (50 ms integrating time, and 100 spectra averaging), 12 s (1000 ms integrating

Optics EXPRESS

time, and 12 spectra averaging) for channel 1 (centered at 365 nm), channel 2 (centered at 532 nm), channel 3 (centered at 660 nm), respectively.

For channel 1 (λ = 365 nm), measurement fluctuations (1σ standard deviation) over 12000 s were found to be 0.95, 0.65, and 1.04 Mm^{-1} for α_{ext}, α_{scat}, and α_{abs}, respectively. Short-term measurement precision for α_{ext}, α_{scat}, and α_{abs} was respectively 0.83, 0.60, and 0.94 Mm^{-1} with a 12 s data acquisition time, and improved further to 0.40, 0.26, and 0.43 Mm^{-1} with averaging over 60 s. For channel 2 (λ = 532 nm), the measurement fluctuations (1σ standard deviation) over 10000 s were found to be 0.19, 0.07, and 0.19 Mm^{-1} for α_{ext}, α_{scat}, and α_{abs}. Short-term precision over 5 s (and 60 s) averaging times were respectively 0.14 (0.04), 0.06 (0.02), and 0.15 (0.04) Mm^{-1}. In like manner, standard deviations of 0.75, 0.93, and 1.10 Mm^{-1} over 14000 s were found for α_{ext}, α_{scat}, and α_{abs} in channel 3 (λ = 660 nm). The corresponding measurement precisions over 12 s (and 60 s) averaging times were 0.53 (0.28), 0.83 (0.44), and 0.93 (0.47) Mm^{-1}. The 3σ detection limit ($LOD_{expected, 3\sigma}$) of each parameter was determined from the Gaussian fitted frequency distribution of the time series measurement [32].

A list of the detection limits and precisions of the three-wavelength CES-albedometer and a comparison with some literature reported instruments are shown in Table 2. For aerosol optical instruments operating in the UV region, the precision of our extinction measurement at λ = 365 nm (0.4 Mm^{-1}) was comparable to Washenfelder et al.'s result with a BBCES instrument [21]. The precision of our absorption measurement was comparable to that of the UV-vis photoacoustic spectrophotometer operating at λ = 364 nm [10]; and the reported precisions for all the parameters (α_{ext}, α_{scat} and α_{abs}) were about 5-10 times better than the CRDS-nephelometer operating at λ = 355 nm [33]. In the green wavelength range, the reported extinction measurement precisions of our instrument were comparable with the CRDS-nephelometer operating at λ = 532 nm [23] and the CAPS albedo monitor operating at λ = 530 nm [26]. The precision of our absorption measurements was better than that reported for a three-wavelength photoacoustic spectrometer [34] and very recent a four wavelength portable PAS system [8], and in accordance with the state-of-the-art precision achieved with a multipass PAS [9]. In the red wavelength range, the precisions of α_{ext} and α_{scat} at λ = 660 nm of our instrument were not as good as the result of CAPS albedo monitor [26], but were low enough for ambient applications. The precisions of α_{abs} at λ = 660 nm of our instrument was better than that reported by Wiegand et al. at λ = 687 nm [10] and Linke et al. at λ = 660 nm [34], and comparable with the recently developed four wavelength portable PAS system [8]. Generally speaking the precisions of our measurements are close to the state-of-the-art performances for aerosol optical properties.

Optics EXPRESS

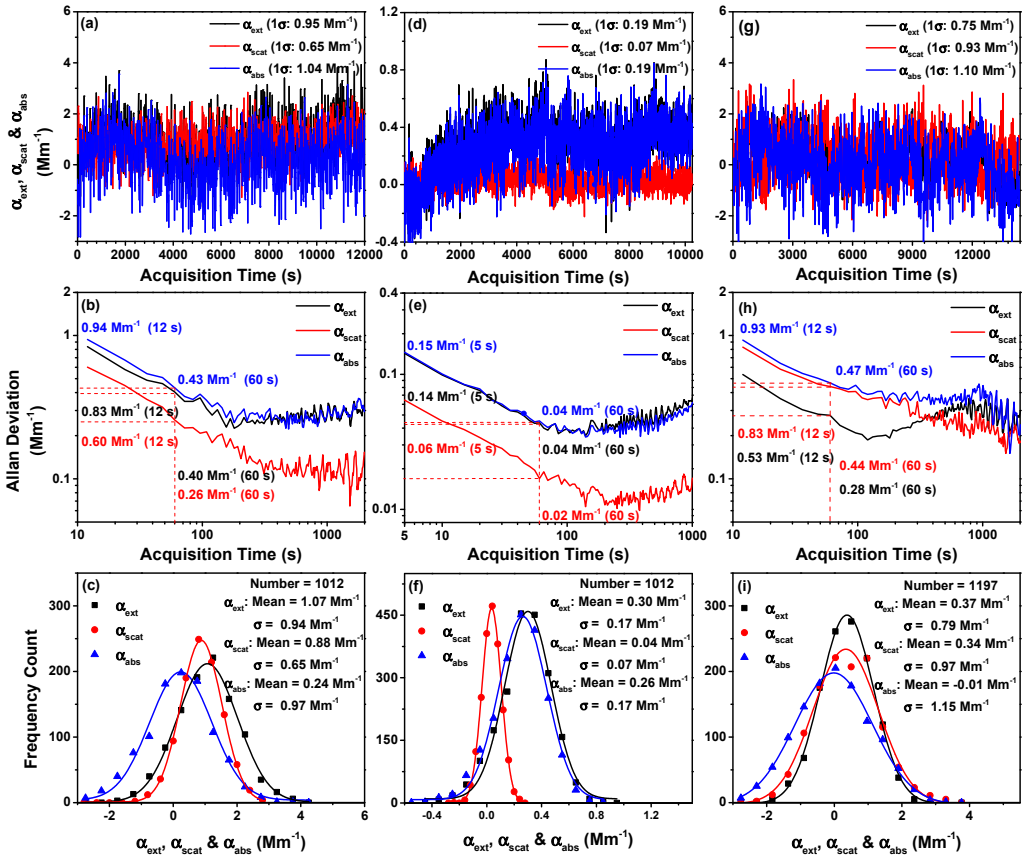


Fig. 3. Performance evaluation of the CES-albedometer. From upper to lower panel: (a)-(c) Channel 1 (λ = 365 nm); (d)-(f) Channel 2 (λ = 532 nm); (g)-(i) Channel 3 (λ = 660 nm) measured with particle free zero air. Measurements time series are shown in the upper panel. The corresponding Allan deviation and frequency distribution of each channel are shown in the middle and lower panels.

Uncertainty contributions associated with the extinction measurement were: mirror reflectivity determination ($1 - R$, < 2.5%), R_L (~0.6%), and particle losses in the optical cavity (~2%). For scattering measurements, uncertainties mainly arose from the scattering calibration factor (K', < 2%), particle losses in the optical cavity (~2%), and the truncated fraction of total scattering (< 1%). Since measurements of the extinction and scattering coefficients were of the same sample, measurement of ω is unaffected by particle losses. The total uncertainties in α_{ext}, α_{scat}, α_{abs}, and ω measurements were estimated to be less than 3.3%, 3.0%, 4.5%, and 5.5%, respectively.

Optics EXPRESS

Table 2. Comparison of precision between three-wavelength CES albedometer and selected literature-reported instruments.

	Parameters	LOD (3σ, Mm^{-1})	Precision (1σ, Mm^{-1})	Literature reported values with other instruments (1 σ)	Reference
Channel 1	α_{ext}(365)	3.89 (12 s)	0.83 (12 s) 0.40 (60 s)	0.21 Mm^{-1} (λ = 365 nm, 60 s) [a] 3.5 Mm^{-1} (λ = 355 nm, 52 s) [b]	21 33
	α_{scat}(365)	2.83 (12 s)	0.60 (12 s) 0.26 (60 s)	3.9 Mm^{-1} (λ = 355 nm, 52 s) [b]	33
	α_{abs}(365)	3.15 (12 s)	0.94 (12 s) 0.43 (60 s)	5.2 Mm^{-1} (λ = 355 nm, 52 s) [b] 0.75 Mm^{-1} (λ = 364 nm, 20 s) [c]	33 10
Channel 2	α_{ext}(532)	0.81 (5 s)	0.14 (5 s) 0.04 (60 s)	0.20 Mm^{-1} (λ = 532 nm, 4 s) [b] 0.05 Mm^{-1} (λ = 530 nm, 60 s) [d]	23 26
	α_{scat}(532)	0.25 (5 s)	0.06 (5 s) 0.02 (60 s)	0.9 Mm^{-1} (λ = 532 nm, 4 s) [b] 0.04 Mm^{-1} (λ = 530 nm, 60 s) [d] 0.9 Mm^{-1} (λ = 546 nm, 20 s) [c]	23 26
	α_{abs}(532)	0.77 (5 s)	0.15 (5 s) 0.04 (60 s)	2.2 Mm^{-1} (λ = 532 nm) [e] 0.31 Mm^{-1} (λ = 532 nm, 120 s) [f] 0.08 Mm^{-1} (λ = 532 nm, 60 s) [h]	10 34 8 9
Channel 3	α_{ext}(660)	2.74 (12 s)	0.53 (12 s) 0.28 (60 s)	0.07 Mm^{-1} (λ = 630 nm, 60 s) [d]	26
	α_{scat}(660)	3.25 (12 s)	0.83 (12 s) 0.44 (60 s)	0.05 Mm^{-1} (λ = 630 nm, 60 s) [d]	26
	α_{abs}(660)	3.46 (12 s)	0.93 (12 s) 0.47 (60 s)	5.1 Mm^{-1} (λ = 687 nm, 20 s) [c] 6.0 Mm^{-1} (λ = 660 nm) [e] 0.38 Mm^{-1} (λ = 662 nm, 120 s) [f]	10 34 8

[a] CES spectrometer; [b] CRDS-nephelometer; [c] UV-Vis photoacoustic spectrometer; [d] CAPS albedo monitor; [e] Three-wavelength single-cell PAS, time not specified; [f] Four wavelength portable single-cell PAS; [h] multipass PAS.

3.2 Wavelength dependent measurement of laboratory-generated aerosols

Aerosol extinction, scattering and absorption coefficients can be calculated from [35]:

$$\alpha_{ext,scat,abs}(\lambda) = \int N(D_p)\frac{\pi}{4}D_p^2 Q_{ext,scat,abs}(m,x,\lambda)dD_p \tag{3}$$

where $N(D_p)$ is the particle number concentration in the size bin dD_p (with mean diameter of D_p). λ is the wavelength of the incident light. m is the complex refractive index (CRI) of the particles ($m = n + ik$, where n and k correspond to the real and imaginary parts of the CRI, respectively). $x = \pi D_p/\lambda$ is the size parameter. $\frac{\pi}{4}D_p^2 Q_{ext,scat,abs}(m,x,\lambda)$ represents the extinction/scattering/absorption cross sections ($\sigma_{ext,scat,abs}$). For chemically homogeneous spherical particles, the extinction, scattering or absorption efficiency can be calculated from Mie theory: $Q_{ext,scat,abs}(m,x,\lambda) = 4\sigma_{ext,scat,abs}/\pi D_p^2$, and vice versa, we can retrieve the CRI of the measured sample from experimental measured efficiencies. The comparison between the

Optics EXPRESS

retrieved CRI with the theoretical value is often used as a common method for evaluating the performance of new aerosol optical instruments [20,21,24,26,28,35–38].

The usual CRI retrieved methods include (1) "the diameter midpoint method", and (2) the entire aerosol size distribution method [39]. The first method is always used for monodisperse (like PSL spheres) or size selected particles, in which an optimization strategy (by varying the values of n and k) is used to find the best fit value with a minimal least-squares deviation (χ^2) of the measured and calculated data [21,24,36]:

$$\chi^2 = \sum_{i=1}^{Num} \frac{(Q_{ext,scat} - Q_{ext,scat_calc})_i^2}{\varepsilon_{Qi}^2} \tag{4}$$

where ε_Q is the standard deviation of the measured Q values. In this method, the CRI can be retrieved with a single optical parameter. However, enough measurements at a set of different diameters are needed to map out the Mie curve and this approach is time consuming. The second method is a new approach used for polydisperse particles. This method incorporates the entire aerosol size distribution into the calculation, and sums up the corresponding extinction or scattering to provide a fast CRI retrieval. Simultaneous measurement of the particle size distribution and at least two optical parameters are required. The merit function can be written as:

$$\chi^2 = \frac{(\alpha_{ext}(\lambda) - \alpha_{ext_calc}(\lambda))^2}{\varepsilon_{\alpha_{ext}(\lambda)}^2} + \frac{(\alpha_{scat}(\lambda) - \alpha_{scat_calc}(\lambda))^2}{\varepsilon_{\alpha_{scat}(\lambda)}^2} \tag{5}$$

where α is the measured extinction or scattering coefficient, ε is the measurement uncertainty, and $\alpha_{calc}(\lambda)$ is the calculated extinction or scattering coefficient binned over all the particle sizes [25,39,40].

$$\alpha_{ext,scat,abs}(\lambda) = \sum N(D_p)\frac{\pi}{4}D_p^2 Q_{ext,scat,abs}(m,x,\lambda) \tag{6}$$

In this work, the performance evaluation of the system was carried out using monodispersed polystyrene latex spheres (PSL, non-absorbing), and three different polydispersed samples, including: ammonium sulfate (AS, CAS 7783-20-2, Sigma Aldrich, non-absorbing), suwannee river fulvic acid (SRFA, IHSS code 1S101F, slightly absorbing, a proxy for light absorbing organic aerosol), and nigrosin (CAS 8005-03-6, Sigma Aldrich, strongly absorbing). The particle generation system was the same as in our previous work [20,24,28]. For PSL particles, the CRIs were retrieved with the first method, and for polydispersed particles, CRIs were retrieved with the second method. The results are discussed as following.

A. PSL

Seven different diameters (200, 240, 300, 350, 400, 450 and 500 nm) of laboratory-generated monodispersed PSL spheres were used for testing the three-wavelength CES-albedometer [20,21,24,26,28]. The plots of α_{ext} and α_{scat} as a function of particle number concentration, as well as plots of Q_{ext} and Q_{scat} versus particle diameters, are shown in Fig. 4.

Optics EXPRESS

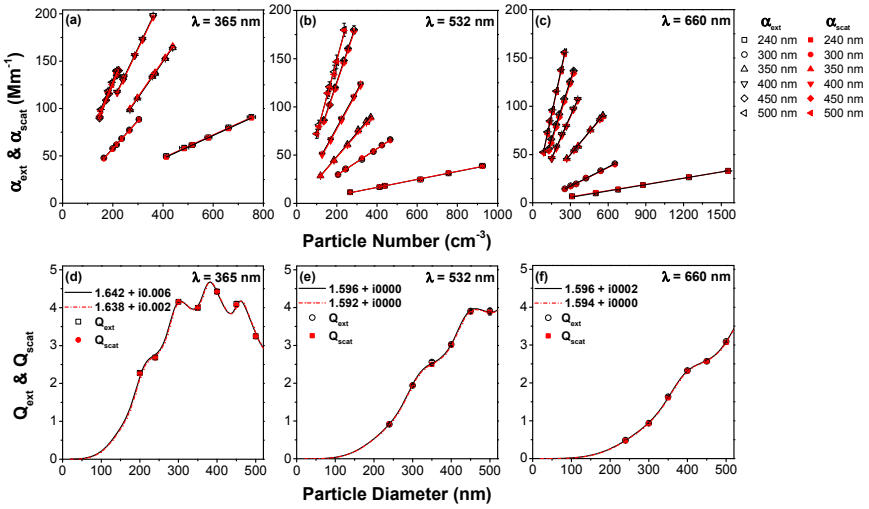


Fig. 4. Upper panel: extinction (solid points) and scattering (hollow points) coefficients as a function of particle number concentration at (a) λ = 365 nm, (b) 532 nm, and (c) 660 nm for monodisperse PSL spheres of 200, 240, 300, 350, 400, 450 and 500 nm diameter. Lower panel: extinction (Q_{ext}, solid points) and scattering (Q_{scat}, hollow points) efficiencies as a function of particle diameter at (d) λ = 365 nm, (e) 532 nm, and (f) 660 nm, respectively. The corresponding Mie theory fit results are shown as solid and dotted lines.

The retrieved CRIs for PSL at 365 nm, 532 nm, and 660 nm from the extinction cross sections were $1.642^{+0.006}_{-0.008}+i0.006^{+0.006}_{-0.006}$, $1.596^{+0.000}_{-0.000}+i0.000^{+0.000}_{-0.000}$, and $1.596^{+0.000}_{-0.000}+i0.002^{+0.000}_{-0.000}$, respectively. The respective CRIs retrieved from the scattering cross sections were $1.638^{+0.022}_{-0.018}+i0.002^{+0.016}_{-0.014}$, $1.592^{+0.000}_{-0.000}+i0.000^{+0.000}_{-0.000}$, and $1.594^{+0.000}_{-0.000}+i0.000^{+0.000}_{-0.000}$. The good agreement between the independently measured extinction and scattering coefficients, and between the resulting CRI values from the extinction and scattering measurements, demonstrate the ability of the three-wavelength CES-albedometer for accurate simultaneous measurement of the extinction and scattering. Figure 5 shows a comparison between the retrieved CRIs at three wavelengths and previously reported results over the UV-visible region. The reported value of n for PSL ranged from ~2.2 to 1.5 and decreased with the wavelength [20,21,24,35–38,41–49]. Excellent agreement was found between our measurements and the literature reported values.

Optics EXPRESS

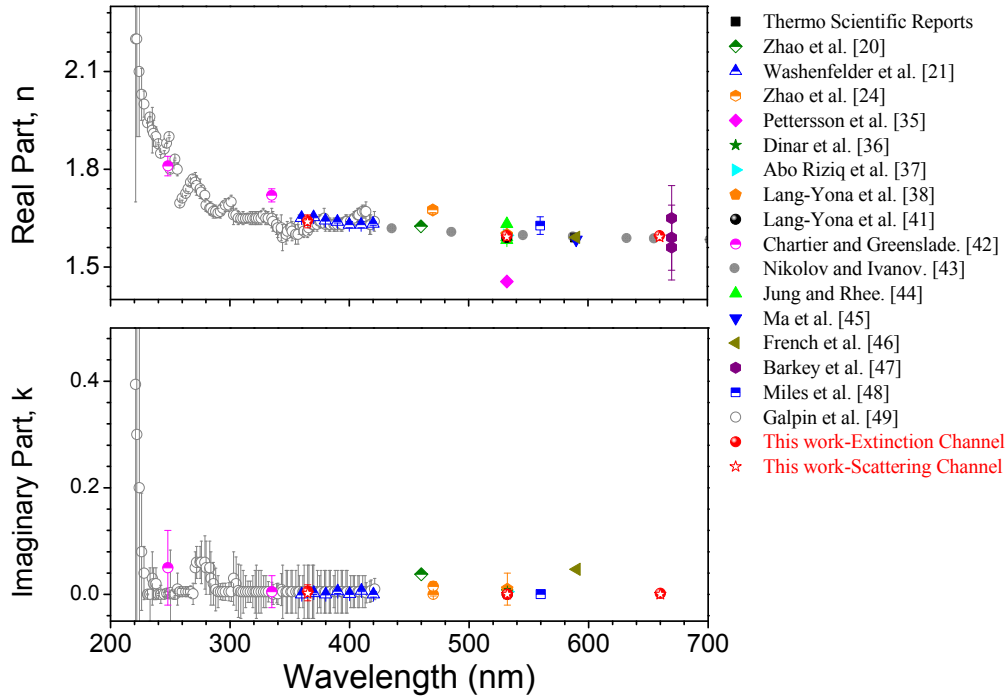


Fig. 5. A comparison of CRI values of PSL particles (upper panel: real part *n*; lower panel: imaginary part *k*) reported in the literature, and those retrieved independently from the scattering and extinction efficiencies in this work.

B. Ammonium sulfate

Ammonium sulfate is a purely scattering species and has negligible absorption in the UV-visible region (i.e., the imaginary part of the CRI, *k*, is close to zero). The measured wavelength dependent extinction, scattering, ω, as well as the corresponding size distribution of the sample are shown in Figs. 6(a) and 6(b). The Ångström exponents of extinction (EAE), scattering (SAE), and absorption coefficients (AAE) were deduced by a power law function ($\alpha_{ext,scat,abs} = a \times \lambda^{-b}$, b = EAE/SAE/AAE) [7,10]. Both extinction and scattering coefficients show a strong wavelength dependence, and the EAE and SAE are both close to 2.5. SAE mainly characterizes aerosol size: a large value of SAE corresponds to small particles generated with a geometric mean diameter less than 100 nm. The values of extinction and scattering coefficients are basically the same, and the values of ω at all three wavelengths are close to 1, in accordance with expectations.

The CRIs of AS retrieved by combining the scattering and extinction coefficients with the aerosol size distribution data were $1.505^{+0.005}_{-0.000}+i0.000^{+0.002}_{-0.000}$, $1.520^{+0.005}_{-0.000}+i0.000^{+0.002}_{-0.000}$, and $1.545^{+0.005}_{-0.000}+i0.002^{+0.000}_{-0.002}$ at λ = 365, 532, and 660 nm, respectively. A comparison of the retrieved CRIs with literature reported values are shown in Fig. 6(c). In the UV spectral region, literature values of *n* ranged from 1.48 to 1.55 [21,36,50–52], and increased with the wavelength (excluding Trainic et al.'s result [51]). The measured CRI values in this study agreed well with Washenfelder et al.'s results (*n* = 1.513 ± 0.004 at λ = 360 nm, *n* = 1.540 ± 0.007 at λ = 420 nm) [21] from their BBCES instrument, and with Flores et al.'s result (1.507 ± 0.024 at λ = 355 nm) [52] using a CRDS instrument and "the diameter midpoint method". The *n* value at λ = 532 nm retrieved in this study is consistent with previously reported values (ranging from 1.51 to 1.55) [35–38,41,50,53]. Our *n* value at λ = 660 nm is slightly larger than the previously reported values in the red region [50], but it is also broadly reasonable.

Optics EXPRESS

The differences between our measurement and Toon et al.'s result (1.525 ± 0.005, λ = 706 nm) [50] was about 1%, which is within the tolerance of the instrumental accuracy.

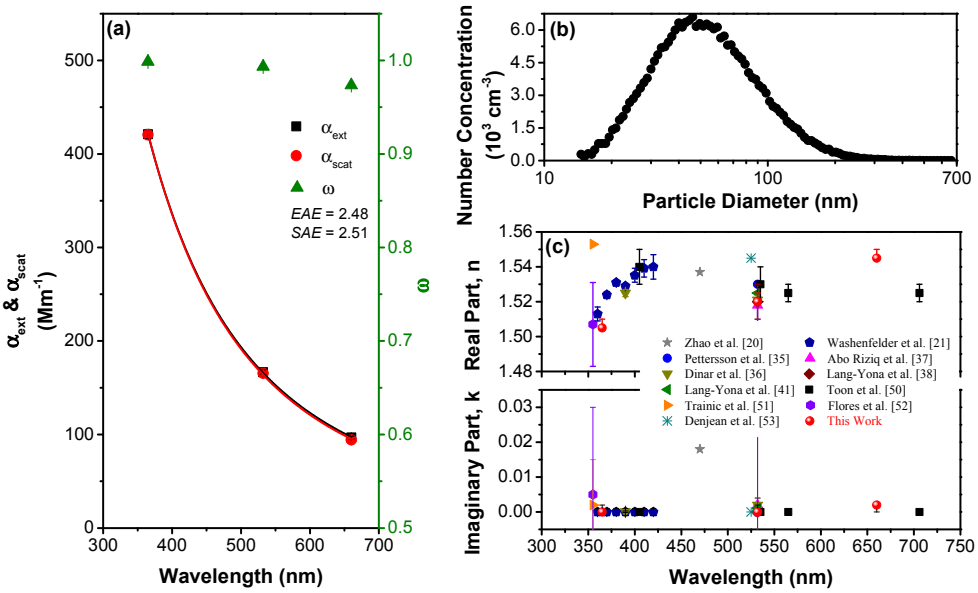


Fig. 6. (a) The measured wavelength-dependent extinction, scattering coefficients and ω of ammonium sulfate, (b) size distribution of the polydispersed sample, and (c) the comparison between the retrieved CRIs and the literature reported values. Error bars are shown where they can be distinguished from the symbol.

C. SRFA

SRFA is a slightly light-absorbing organic substance with an obvious absorption spectrum in the UV-visible region. It is often used as a proxy material for brown carbon [54,22]. The wavelength-dependent extinction, scattering, absorption, and ω are shown in Fig. 7(a). The measured ω values were 0.80 ± 0.01, 0.93 ± 0.02, 0.98 ± 0.02 at λ = 365, 532, and 660 nm, in reasonable agreement with the values reported by Bluvshtein et al. (0.88 ± 0.03, 0.95 ± 0.03, 0.97 ± 0.03 at λ = 365, 532, 660 nm) [22]. The fitted EAE, SAE, AAE were about 2.9, 2.6, and 6.1. The measured AAE is consistent with the result reported previously by Phillips and Smith (~6) [55].

The retrieved CRIs of SRFA aerosol were $1.580^{+0.000}_{-0.005}+i0.038^{+0.004}_{-0.002}$ at λ = 365 nm, $1.580^{+0.000}_{-0.005}+i0.008^{+0.002}_{-0.004}$ at λ = 532 nm, and $1.605^{+0.005}_{-0.005}+i0.002^{+0.002}_{-0.002}$ at λ = 660 nm. The measured *n* values are lower than those of Washenfelder et al.'s [21] and Bluvshtein et al.'s [22], but comparable with the *n* values reported by Flores et al. [56]. This discrepancy may arise from the different size distribution of SRFA particles used in different studies. However, the spectral behavior of *k* is consistent with Bluvshtein et al.'s result [22]. The reported *k* values are generally consistent with previous studies [21,22,56].

Optics EXPRESS

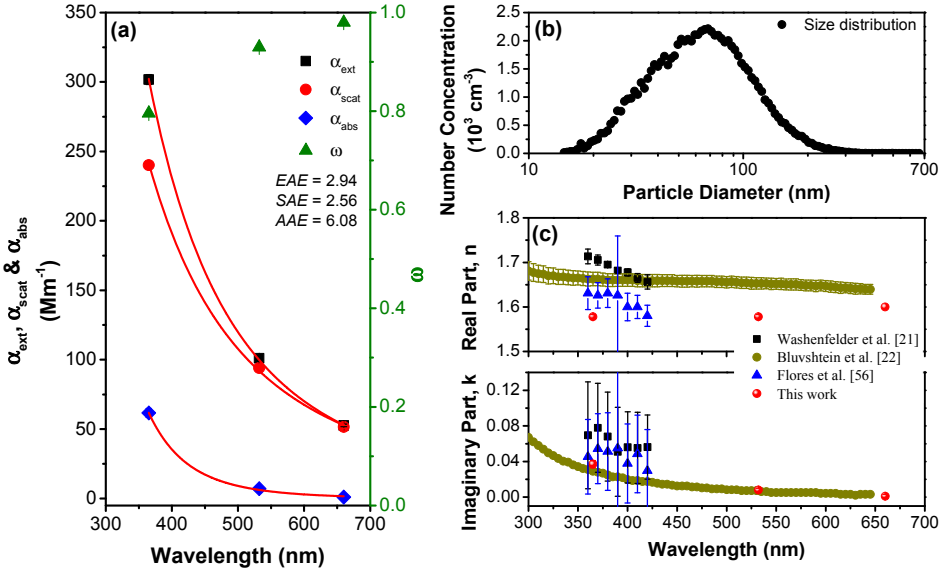


Fig. 7. (a) The measured wavelength-dependent extinction, scattering, absorption coefficients, and ω, (b) the corresponding size distribution of the sample, and (c) the retrieved CRI values of SRFA aerosol from this work and previous studies. Error bars are shown where they can be distinguished from the symbol.

D. Nigrosin

Nigrosin is a strongly light-absorbing black dye with strong absorption peaks in the UV and green spectral regions [10,57]. Nigrosin is frequently used as a standard sample to validate various aerosol absorption measurement instruments [9,10]. The wavelength-dependent absorption measurements made with the three-wavelength CES-albedometer are shown in Fig. 8(a). The measured ω were 0.605 ± 0.005 at λ = 365 nm, 0.359 ± 0.005 at λ = 532 nm, and 0.498 ± 0.010 at λ = 660 nm. The corresponding CRIs retrieved in this study were $1.580^{+0.000}_{-0.005}+i0.110^{+0.006}_{-0.004}$, $1.575^{+0.005}_{-0.005}+i0.212^{+0.010}_{-0.006}$ and $1.870^{+0.010}_{-0.010}+i0.186^{+0.008}_{-0.010}$, respectively.

In the UV spectral region, our retrieved *n* value was consistent with the reported value by Flores et al. [52] (1.568 ± 0.056) at λ = 355 nm. The retrieved *k* value at λ = 365 nm is consistent with those reported values by Washenfelder et al. [21] and Bluvshtein et al. [57]. At λ = 532 nm, the measured CRI value was mostly consistent with the reported values by Dinar et al. (1.649 (± 0.007) + *i* 0.238 (± 0.05)) [36], Lang-Yona et al. (1.65 (± 0.01) + *i* 0.24 (± 0.01)) [38], Lack et al. (1.70 (± 0.04) + *i* 0.31 (± 0.05)) [9], and Flores et al. (1.626 (± 0.021) + *i* 0.243 (± 0.023)) [52]. At 660 nm, the *n* value reported here was consistent with Bluvshtein et al.'s result [57], but larger than the reported value (n = 1.67) by Garvey et al. at λ = 630 nm [58].

Optics EXPRESS

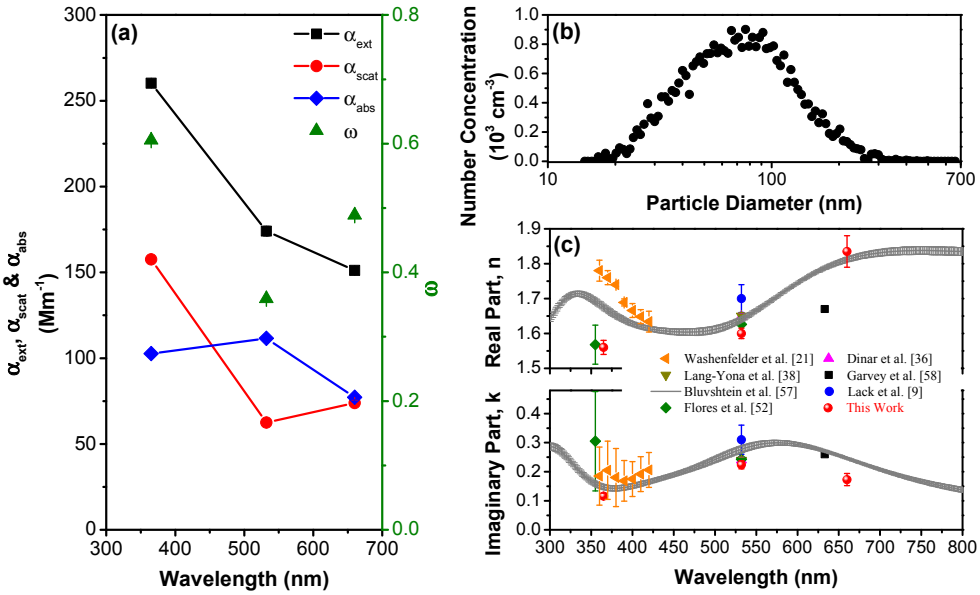


Fig. 8. (a) The measured wavelength-dependent extinction, scattering, absorption coefficients, and ω, (b) size distribution of the sample, and (c) the retrieved *m* of nigrosin aerosol and its comparison with previously reported results. Error bars are shown where they can be distinguished from the symbol.

Overall, the reported CRI values of AS, SRFA, and nigrosine in this work are consistent with previous measurements, demonstrating the accuracy of the three-wavelength CES-albedometer for measurement of multiple optical parameters.

4. Conclusion

In this paper, we report the development and characterization of a three-wavelength cavity-enhanced albedometer for the simultaneous in situ measurements of multiple optical parameters across the UV-visible spectral region. Laboratory generated monodisperse PSL spheres, as well as polydisperse AS, SRFA, and nigrosine aerosols were used for the performance evaluation of the instrument. The retrieved wavelength-dependent CRIs shown close agreement with previous reports in the literature, demonstrating accuracy of the spectrum measurements of extinction, scattering, absorption, and ω. The short wavelength measurements are particularly valuable for identifying BrC and other organic light absorbing species, and for distinguishing the absorption of BrC from BC because BrC absorption is only significant at shorter wavelengths [59,60]. The LED based three-wavelength CES-albedometer offers a valuable, potential low cost and portability method for aerosol optical measurement, which will provide high-quality data for aerosol classification research under ambient condition.

Funding

National Natural Science Foundation of China (41330424); Natural Science Foundation of Anhui Province (1508085J03); and Youth Innovation Promotion Association of the Chinese Academy of Sciences (CAS) (2016383).

References

1. H. Yu, Y. J. Kaufman, M. Chin, G. Feingold, L. A. Remer, T. L. Anderson, Y. Balkanski, N. Bellouin, O. Boucher, S. Christopher, P. DeCola, R. Kahn, D. Koch, N. Loeb, M. S. Reddy, M. Schulz, T. Takemura, and M. Zhou, "A review of measurement-based assessments of the aerosol direct radiative effect and forcing," Atmos. Chem. Phys. **6**(3), 613–666 (2006).

Optics EXPRESS

2. P. B. Russell, R. W. Bergstrom, Y. Shinozuka, A. D. Clarke, P. F. DeCarlo, J. L. Jimenez, J. M. Livingston, J. Redemann, O. Dubovik, and A. Strawa, "Absorption Angstrom Exponent in AERONET and related data as an indicator of aerosol composition," Atmos. Chem. Phys. **10**(3), 1155–1169 (2010).
3. R. W. Bergstrom, P. Pilewskie, P. B. Russell, J. Redemann, T. C. Bond, P. K. Quinn, and B. Sierau, "Spectral absorption properties of atmospheric aerosols," Atmos. Chem. Phys. **7**(23), 5937–5943 (2007).
4. J. Li, B. E. Carlson, and A. A. Lacis, "Using single-scattering albedo spectral curvature to characterize East Asian aerosol mixtures," J. Geophys. Res. Atmos. **120**(5), 2037–2052 (2015).
5. R. Bahadur, P. S. Praveen, Y. Xu, and V. Ramanathan, "Solar absorption by elemental and brown carbon determined from spectral observations," Proc. Natl. Acad. Sci. U.S.A. **109**(43), 17366–17371 (2012).
6. P. B. Russell, M. Kacenelenbogen, J. M. Livingston, O. P. Hasekamp, S. P. Burton, G. L. Schuster, M. S. Johnson, K. D. Knobelspiesse, J. Redemann, S. Ramachandran, and B. Holben, "A multiparameter aerosol classification method and its application to retrievals from spaceborne polarimetry," J. Geophys. Res. Atmos. **119**(16), 9838–9863 (2014).
7. H. Moosmüller, R. K. Chakrabarty, and W. P. Arnott, "Aerosol light absorption and its measurement: A review," J. Quant. Spectrosc. Radiat. Transf. **110**(11), 844–878 (2009).
8. D. A. Fischer and G. D. Smith, "A portable, four-wavelength, single-cell photoacoustic spectrometer for ambient aerosol absorption," Aerosol Sci. Technol. **52**(4), 393–406 (2018).
9. D. A. Lack, E. R. Lovejoy, T. Baynard, A. Pettersson, and A. R. Ravishankara, "Aerosol absorption measurement using photoacoustic spectroscopy: Sensitivity, calibration, and uncertainty developments," Aerosol Sci. Technol. **40**(9), 697–708 (2006).
10. J. R. Wiegand, L. D. Mathews, and G. D. Smith, "A UV-Vis photoacoustic spectrophotometer," Anal. Chem. **86**(12), 6049–6056 (2014).
11. C. Haisch, P. Menzenbach, H. Bladt, and R. Niessner, "A wide spectral range photoacoustic aerosol absorption spectrometer," Anal. Chem. **84**(21), 8941–8945 (2012).
12. J. G. Radney and C. D. Zangmeister, "Measurement of gas and aerosol phase absorption spectra across the visible and near-IR using supercontinuum photoacoustic spectroscopy," Anal. Chem. **87**(14), 7356–7363 (2015).
13. N. Sharma, I. J. Arnold, H. Moosmüller, W. P. Arnott, and C. Mazzoleni, "Photoacoustic and nephelometric spectroscopy of aerosol optical properties with a supercontinuum light source," Atmos. Meas. Tech. **6**(12), 3501–3513 (2013).
14. J. M. Langridge, M. S. Richardson, D. Lack, D. Law, and D. M. Murphy, "Aircraft instrument for comprehensive characterization of aerosol optical properties, Part I: wavelength-dependent optical extinction and its relative humidity dependence measured using cavity ringdown spectroscopy," Aerosol Sci. Technol. **45**(11), 1305–1318 (2011).
15. S. E. Fiedler, A. Hese, and A. A. Ruth, "Incoherent broad-band cavity-enhanced absorption spectroscopy," Chem. Phys. Lett. **371**(3–4), 284–294 (2003).
16. J. E. Thompson and H. D. Spangler, "Tungsten source integrated cavity output spectroscopy for the determination of ambient atmospheric extinction coefficient," Appl. Opt. **45**(11), 2465–2473 (2006).
17. M. Dong, W. Zhao, Y. Cheng, C. Hu, X. Gu, and W. Zhang, "Incoherent broadband cavity enhanced absorption spectroscopy for trace gases detection and aerosol extinction measurement," Wuli Xuebao **61**(6), 06072 (2012).
18. R. M. Varma, S. M. Ball, T. Brauers, H.-P. Dorn, U. Heitmann, R. L. Jones, U. Platt, D. Pöhler, A. A. Ruth, A. J. L. Shillings, J. Thieser, A. Wahner, and D. S. Venables, "Light extinction by secondary organic aerosol: an intercomparison of three broadband cavity spectrometers," Atmos. Meas. Tech. **6**(11), 3115–3130 (2013).
19. A. A. Ruth, S. Dixneuf, and R. Raghunandan, "Broadband cavity enhanced absorption spectroscopy with incoherent light," in Cavity-Enhanced Spectroscopy and Sensing, G. Gagliardi and H. P. Loock, eds., Vol. 179 of Series Springer Series in Optical Sciences (2014), pp 485–517.
20. W. Zhao, M. Dong, W. Chen, X. Gu, C. Hu, X. Gao, W. Huang, and W. Zhang, "Wavelength-resolved optical extinction measurements of aerosols using broad-band cavity-enhanced absorption spectroscopy over the spectral range of 445-480 nm," Anal. Chem. **85**(4), 2260–2268 (2013).
21. R. A. Washenfelder, J. M. Flores, C. A. Brock, S. S. Brown, and Y. Rudich, "Broadband measurements of aerosol extinction in the ultraviolet spectral region," Atmos. Meas. Tech. **6**(4), 861–877 (2013).
22. N. Bluvshtein, J. M. Flores, L. Segev, and Y. Rudich, "A new approach for retrieving the UV–vis optical properties of ambient aerosols," Atmos. Meas. Tech. **9**(8), 3477–3490 (2016).
23. J. E. Thompson, N. Barta, D. Policarpio, and R. Duvall, "A fixed frequency aerosol albedometer," Opt. Express **16**(3), 2191–2205 (2008).
24. W. Zhao, X. Xu, M. Dong, W. Chen, X. Gu, C. Hu, Y. Huang, X. Gao, W. Huang, and W. Zhang, "Development of a cavity-enhanced aerosol albedometer," Atmos. Meas. Tech. **7**(8), 2551–2566 (2014).
25. X. Xu, W. Zhao, Q. Zhang, S. Wang, B. Fang, W. Chen, D. S. Venables, X. Wang, W. Pu, X. Wang, X. Gao, and W. Zhang, "Optical properties of atmospheric fine particles near Beijing during the HOPE-J^{3}A campaign," Atmos. Chem. Phys. **16**(10), 6421–6439 (2016).
26. T. B. Onasch, P. Massoli, P. L. Kebabian, F. B. Hills, F. W. Bacon, and A. Freedman, "Single scattering albedo monitor for airborne particulates," Aerosol Sci. Technol. **49**(4), 267–279 (2015).
27. Y. Wei, L. Ma, T. Cao, Q. Zhang, J. Wu, P. R. Buseck, and J. E. Thompson, "Light scattering and extinction measurements combined with laser-induced incandescence for the real-time determination of soot mass absorption cross section," Anal. Chem. **85**(19), 9181–9188 (2013).

Optics EXPRESS

28. W. Zhao, X. Xu, B. Fang, Q. Zhang, X. Qian, S. Wang, P. Liu, W. Zhang, Z. Wang, D. Liu, Y. Huang, D. S. Venables, and W. Chen, "Development of an incoherent broad-band cavity-enhanced aerosol extinction spectrometer and its application to measurement of aerosol optical hygroscopicity," Appl. Opt. **56**(11), E16–E22 (2017).
29. J. M. Langridge, M. S. Richardson, D. L. Lack, C. A. Brock, and D. M. Murphy, "Limitations of the photoacoustic technique for aerosol absorption measurement at high relative humidity," Aerosol Sci. Technol. **47**(11), 1163–1173 (2013).
30. R. Varma, H. Moosmüller, and W. P. Arnott, "Toward an ideal integrating nephelometer," Opt. Lett. **28**(12), 1007–1009 (2003).
31. A. W. Strawa, R. Castaneda, T. Owano, D. S. Baer, and B. A. Paldus, "The measurement of aerosol optical properties using continuous wave cavity ring-down techniques," J. Atmos. Ocean. Technol. **20**(4), 454–465 (2003).
32. B. Fang, W. Zhao, X. Xu, J. Zhou, X. Ma, S. Wang, W. Zhang, D. S. Venables, and W. Chen, "Portable broadband cavity-enhanced spectrometer utilizing Kalman filtering: application to real-time, in situ monitoring of glyoxal and nitrogen dioxide," Opt. Express **25**(22), 26910–26922 (2017).
33. L. Ma and J. E. Thompson, "Optical properties of dispersed aerosols in the near ultraviolet (355 nm): measurement approach and initial data," Anal. Chem. **84**(13), 5611–5617 (2012).
34. C. Linke, I. Ibrahim, N. Schleicher, R. Hitzenberger, M. O. Andreae, T. Leisner, and M. Schnaiter, "A novel single cavity three-wavelength photoacoustic spectrometer for atmospheric aerosol research," Atmos. Meas. Tech. **9**(11), 5331–5346 (2016).
35. A. Pettersson, E. R. Lovejoy, C. A. Brock, S. S. Brown, and A. R. Ravishankara, "Measurement of aerosol optical extinction at with pulsed cavity ring down spectroscopy," J. Aerosol Sci. **35**(8), 995–1011 (2004).
36. E. Dinar, A. A. Riziq, C. Spindler, C. Erlick, G. Kiss, and Y. Rudich, "The complex refractive index of atmospheric and model humic-like substances (HULIS) retrieved by a cavity ring down aerosol spectrometer (CRD-AS)," Faraday Discuss. **137**, 279–318 (2008).
37. A. Abo Riziq, C. Erlick, E. Dinar, and Y. Rudich, "Optical properties of absorbing and non-absorbing aerosols retrieved by cavity ring down (CRD) spectroscopy," Atmos. Chem. Phys. **7**(6), 1523–1536 (2007).
38. N. Lang-Yona, Y. Rudich, E. Segre, E. Dinar, and A. Abo-Riziq, "Complex refractive indices of aerosols retrieved by continuous wave-cavity ring down aerosol spectrometer," Anal. Chem. **81**(5), 1762–1769 (2009).
39. C. Spindler, A. A. Riziq, and Y. Rudich, "Retrieval of aerosol complex refractive index by combining cavity ring down aerosol spectrometer measurements with full size distribution information," Aerosol Sci. Technol. **41**(11), 1011–1017 (2007).
40. L. A. Mack, E. J. T. Levin, S. M. Kreidenweis, D. Obrist, H. Moosmüller, K. A. Lewis, W. P. Arnott, G. R. McMeeking, A. P. Sullivan, C. E. Wold, W.-M. Hao, J. L. Collett, Jr., and W. C. Malm, "Optical closure experiments for biomass smoke aerosols," Atmos. Chem. Phys. **10**(18), 9017–9026 (2010).
41. N. Lang-Yona, A. Abo-Riziq, C. Erlick, E. Segre, M. Trainic, and Y. Rudich, "Interaction of internally mixed aerosols with light," Phys. Chem. Chem. Phys. **12**(1), 21–31 (2010).
42. R. T. Chartier and M. E. Greenslade, "Initial investigation of the wavelength dependence of optical properties measured with a new multi-pass Aerosol Extinction Differential Optical Absorption Spectrometer (AE-DOAS)," Atmos. Meas. Tech. **5**(4), 709–721 (2012).
43. I. D. Nikolov and C. D. Ivanov, "Optical plastic refractive measurements in the visible and the near-infrared regions," Appl. Opt. **39**(13), 2067–2070 (2000).
44. C. Jung and B. K. Rhee, "Simultaneous determination of thickness and optical constants of polymer thin film by analyzing transmittance," Appl. Opt. **41**(19), 3861–3865 (2002).
45. X. Ma, J. Q. Lu, R. S. Brock, K. M. Jacobs, P. Yang, and X. H. Hu, "Determination of complex refractive index of polystyrene microspheres from 370 to 1610 nm," Phys. Med. Biol. **48**(24), 4165–4172 (2003).
46. R. H. French, K. I. Winey, M. K. Yang, and W. M. Qiu, "Optical properties and Van Der Waals-London dispersion interactions of polystyrene determined by vacuum ultraviolet spectroscopy and spectroscopic ellipsometry," Aust. J. Chem. **60**(4), 251–263 (2007).
47. B. Barkey, S. E. Paulson, and A. Chung, "Genetic algorithm inversion of dual polarization polar nephelometer data to determine aerosol refractive index," Aerosol Sci. Technol. **41**(8), 751–760 (2007).
48. R. E. H. Miles, S. Rudić, A. J. Orr-Ewing, and J. P. Reid, "Influence of uncertainties in the diameter and refractive index of calibration polystyrene beads on the retrieval of aerosol optical properties using cavity ring down spectroscopy," J. Phys. Chem. A **114**(26), 7077–7084 (2010).
49. T. Galpin, R. T. Chartier, N. Levergood, and M. E. Greenslade, "Refractive index retrievals for polystyrene latex spheres in the spectral range 220–420 nm," Aerosol Sci. Technol. **51**(10), 1158–1167 (2017).
50. O. B. Toon, J. B. Pollack, and B. N. Khare, "The optical constants of several atmospheric aerosol species: Ammonium sulfate, aluminum oxide, and sodium chloride," J. Geophys. Res. Atmos. **81**(33), 5733–5748 (1976).
51. M. Trainic, A. Abo Riziq, A. Lavi, J. M. Flores, and Y. Rudich, "The optical, physical and chemical properties of the products of glyoxal uptake on ammonium sulfate seed aerosols," Atmos. Chem. Phys. **11**(18), 9697–9707 (2011).
52. J. Michel Flores, R. Z. Bar-Or, N. Bluvshtein, A. Abo-Riziq, A. Kostinski, S. Borrmann, I. Koren, I. Koren, and Y. Rudich, "Absorbing aerosols at high relative humidity: linking hygroscopic growth to optical properties," Atmos. Chem. Phys. **12**(12), 5511–5521 (2012).

Optics EXPRESS

53. C. Denjean, P. Formenti, B. Picquet-Varrault, Y. Katrib, E. Pangui, P. Zapf, and J. F. Doussin, "A new experimental approach to study the hygroscopic and optical properties of aerosols: application to ammonium sulfate particles," Atmos. Meas. Tech. **7**(1), 183–197 (2014).
54. P. F. Liu, N. Abdelmalki, H.-M. Hung, Y. Wang, W. H. Brune, and S. T. Martin, "Ultraviolet and visible complex refractive indices of secondary organic material produced by photooxidation of the aromatic compounds toluene and m-xylene," Atmos. Chem. Phys. **15**(3), 1435–1446 (2015).
55. S. M. Phillips and G. D. Smith, "Light absorption by charge transfer complexes in brown carbon aerosols," Environ. Sci. Technol. Lett. **1**(10), 382–386 (2014).
56. J. M. Flores, R. A. Washenfelder, G. Adler, H. J. Lee, L. Segev, J. Laskin, A. Laskin, S. A. Nizkorodov, S. S. Brown, and Y. Rudich, "Complex refractive indices in the near-ultraviolet spectral region of biogenic secondary organic aerosol aged with ammonia," Phys. Chem. Chem. Phys. **16**(22), 10629–10642 (2014).
57. N. Bluvshtein, J. M. Flores, Q. He, E. Segre, L. Segev, N. Hong, A. Donohue, J. N. Hilfiker, and Y. Rudich, "Calibration of a multi-pass photoacoustic spectrometer cell using light-absorbing aerosols," Atmos. Meas. Tech. **10**(3), 1203–1213 (2017).
58. D. M. Garvey and R. G. Pinnick, "Response characteristics of the particle measuring systems Active Scattering Aerosol Spectrometer Probe (ASASP-X)," Aerosol Sci. Technol. **2**(4), 477–488 (1983).
59. T. W. Kirchstetter, T. Novakov, and P. V. Hobbs, "Evidence that the spectral dependence of light absorption by aerosols is affected by organic carbon," J. Geophys. Res. **109**, 21208 (2004).
60. M. O. Andreae and A. Gelencser, "Black carbon or brown carbon? The nature of light-absorbing carbonaceous aerosols," Atmos. Chem. Phys. **6**(10), 3131–3148 (2006).

143.239.102.117 {ts '2019-03-26 06:33:53'}